Geophysical transects in the Abitibi greenstone belt of Canada from the mineral-exploration-oriented Metal Earth project

Article *in* The Leading Edge · April 2023

DOI: 10.1190/tle42040245.1

CITATIONS
0

READS
74

18 authors, including:

Richard Stuart Smith
Laurentian University
177 PUBLICATIONS **3,243** CITATIONS
SEE PROFILE

Rajesh Vayavur
Laurentian University
13 PUBLICATIONS **85** CITATIONS
SEE PROFILE

Graham J. Hill
University of Canterbury
53 PUBLICATIONS **1,197** CITATIONS
SEE PROFILE

David B. Snyder
Laurentian University
6 PUBLICATIONS **26** CITATIONS
SEE PROFILE

Geophysical transects in the Abitibi greenstone belt of Canada from the mineral-exploration-oriented Metal Earth project

Richard S. Smith[1], Mostafa Naghizadeh[2], Saeid Cheraghi[1], Ademola Adetunji[1], Rajesh Vayavur[1], Esmaeil Eshaghi[3], Graham J. Hill[4], David Snyder[1], Eric A. Roots[1], Fabiano Della Justina[1], Hossein Jodeiri Akbari Fam[1], Christopher Mancuso[1], William McNeice[5], Amir Maleki[6], Rasmus Haugaard[1], Taus R. C. Jørgensen[1], P. E. Wannamaker[†], and V. Maris[7]

https://doi.org/10.1190/tle42040245.1

Abstract

The Metal Earth project integrates geophysics, geology, geochemistry, and geochronology to improve the understanding of metal endowment in Precambrian terranes. Magnetics (airborne), gravity, magnetotellurics, and reflection seismic methods are the primary geophysical tools employed. Data were collected along 13 transects in the initial phase of the project. All geophysical tools are crucial for understanding the structure of the shallow, middle, and deeper crust and identifying pathways along which the constituents of critical minerals might have migrated from a source to a deposit. The magnetic data are used predominantly to help map the geology away from the transects, and the gravity data are useful for extending the near-surface geology to depths up to 8 km. The magnetotelluric data show the upper Archean crust to about 10 km as highly resistive, except for some conductive subvertical zones that correspond to major deformation zones, many of which are known to be metalliferous. This suggests that these conductive zones could have been hydrothermal fluid pathways feeding the mineral deposits. These zones can be traced to larger horizontal conductive zones in the midcrust. The seismic reflection data are consistent with and complement this: the upper crust is primarily nonreflective; however, the midcrust shows many horizontal reflectors, usually with a consistent dip to the north. Processing crooked-line seismic data is problematic, and techniques have been developed to improve the imaging, including multifocusing, 3D processing, full-waveform inversion, and cross-dip moveout methods. Passive seismic data have also been collected. Ambient-noise surface-wave tomography can be used to infer broad zones of similar seismic velocity between major reflectors, while receiver function analysis has been used to identify deeper structures such as horizontal features at or below the Moho and a dipping structure evident to about 70 km depth.

Introduction

The Metal Earth project was funded by the Canadian Government through the Canada First Research Excellence Fund in 2017 to help understand why mineral resources critical for our society are plentiful in some (more endowed) locations but are less plentiful in other (less endowed) locations. The initial stage of the project was structured to focus on 13 transects, some more endowed, some less endowed, and to study the differences between the two so that the characteristics of the well-endowed locations are understood and can be used to design programs to explore for critical minerals. The locations of the 10 main transects are shown in Figure 1.

The transects were located in the Abitibi and Wabigoon subprovinces of the Superior Province of the Canadian Precambrian

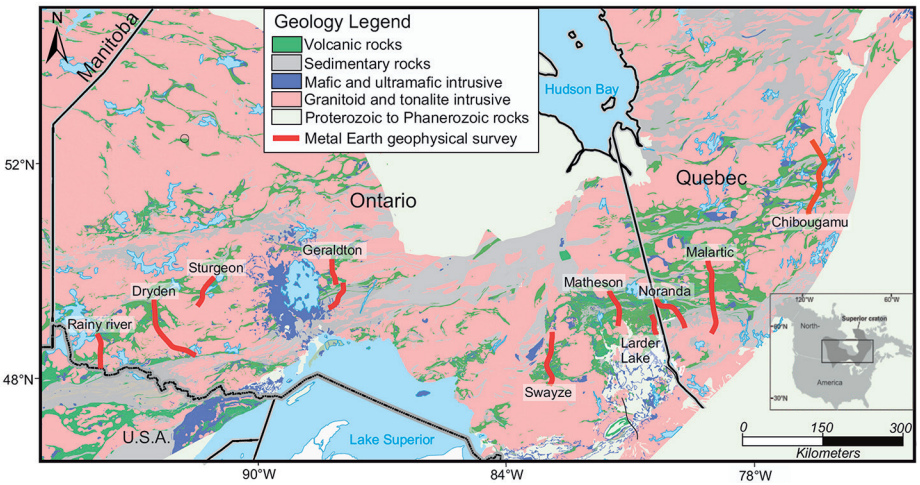

Figure 1. Geology of the southern Superior Province and location of 10 of the main transects (red lines). The geology is greatly simplified with the protolith being specified, although all rocks are metamorphosed to variable extents.

[1]Laurentian University, Harquail School of Earth Sciences, Sudbury, Ontario, Canada. E-mail: rssmith@laurentian.ca; scheraghi@laurentian.ca; aadetunji@laurentian.ca; rvayavur@laurentian.ca; dbsnyder1867@gmail.com; eroots@laurentian.ca; fjustina@laurentian.ca; hjodeiri@laurentian.ca; cmancuso@laurentian.ca; rnielsen@laurentian.ca; tx_joergensen@laurentian.ca.
[2]OptiSeis Solutions Ltd., Calgary, Alberta, Canada. E-mail: mostafa.naghizadeh@optiseis.com.
[3]Fortescue Metals Group, East Perth, Australia. E-mail: eshaghi.es@gmail.com.
[4]Czech Academy of Sciences, Prague, Czech Republic. E-mail: gjhill@ig.cas.cz.
[5]Discovery Geophysics International, Vancouver, British Columbia, Canada. E-mail: wmcneice20@gmail.com.
[6]Wallbridge Mining Company, Sudbury, Ontario, Canada. E-mail: malekiamir3034@gmail.com.
[7]University of Utah, Energy and Geoscience Institute, Salt Lake City, Utah, USA. E-mail: vmaris@egi.utah.edu.
[†]Deceased.

Shield. The Swayze to Chibougamau transects are in the Abitibi, and the Rainy River to Geraldton transects are in the Wabigoon. The geology and ages (circa 2.7 Ga) of the volcanic rocks in these two subprovinces are quite similar. The four transects between Matheson to Malartic (inclusive) are considered to be far better endowed than the others. Ideally, the geometry of each transect would be a straight line perpendicular to the strike of the exposed geology in the area. Practically, however, the strike of the geology changes rapidly, and the transects were restricted to public roads and logging roads. As a result, the transects are usually crooked.

The project is multidisciplinary. Besides geophysics, it involves geologic mapping and sampling, geochemical analysis, and geochronology (e.g., Mole et al., 2021). In a typical year, about 170 geoscientists are working on the project, with many of these contributing over multiple years.

The geologic mapping includes determining the metamorphic history, hydrothermal alteration processes, and economically important geologic structures. Public-domain aeromagnetic data, available from the Ontario Geological Survey, were an important part of improving the geologic maps and identifying and extending geologic structures (e.g., Maleki et al., 2021). The mapping, sampling, and geochemical analyses generally are restricted to rocks at or close to the surface, so geophysical data are important to extend the geology to depth and to identify structures in the crust that might have been pathways taken by the constituents of critical mineral deposits (metals) from the source to deposition sites. The key metals in critical minerals are (1) nickel, cobalt, and platinum group elements, which often are associated with mafic or ultramafic rocks; (2) copper and zinc, often which are associated with volcanic rocks; and (3) rare earth elements in intrusive rocks, which are common in the Superior Province. There are also many gold deposits in the study area, and these occur close to major structures within or adjacent to volcanic rocks.

This paper is a review of work that has been published recently, or is in press, so it represents only a fraction of the work done thus far on the project. Space constraints mean that even some of the published work has not been summarized; however, citations to these works are given for those interested in further reading.

Geophysical data acquisition and compilation

Reflection seismic data were acquired along the crooked-line transects in three modes (Naghizadeh et al., 2019). A regional mode extended along the length of the transect with 50 m source spacing, 25 m geophone spacing, and an effective bandwidth of both source and sensors from 3 to 96 Hz. The sources were four vibroseis trucks. The length of the correlated seismic trace was 12 s, allowing features to be identified down to about 36 km. With some effort, the correlation processing of the data could be applied to the lower frequencies to extend the sections a few additional seconds to image the base of the crust. A more detailed mode was used with a bandwidth of 5–120 Hz, a geophone spacing of 12.5 m, and an effective source spacing of 25 m. The correlated trace length was 12 s, but only 4 s was studied because this detailed mode was intended to resolve shallower features in the top 12 km occupied by the upper crust (Cheraghi et al., 2020). A long-offset mode was acquired on select regional transects where geophones spread along the entire transect were used to simultaneously record long-offset data for the purposes of undertaking refraction processing and full-waveform inversion (Villamizar et al., 2022).

Passive seismic data were also acquired on the Larder Lake transect (Naghizadeh et al., 2022), situated in one of the relatively well-endowed areas. This survey used 40 broadband multicomponent seismometers to measure the natural seismic signals with a station spacing of approximately 1 km. In all, 22 teleseismic events with magnitude greater than 5 were identified and used in receiver function analysis (Ammon, 1991) to generate a P-to-S wave convertibility section to 70 km depth. Passive surface-wave data can also be extracted from the same data and used in ambient-noise surface-wave tomography (Campillo, 2006) to estimate the S-wave velocity section to about 10 km depth.

Passive electromagnetic data were also collected along the transects (Hill et al., 2021). These were primarily broadband magnetotelluric (BBMT) data, which are time-varying magnetic and electric fields at stations spaced approximately 5 km apart along the transects. However, a number of stations were collected beyond the extent of the transects and on either side of the transects to help constrain the 3D structure beneath the transects. These stations were occupied for one to two days and acquired data in the frequency range 0.001–320 Hz. Like the more detailed seismic sections, there are also more detailed magnetotelluric (MT) sections where stations are approximately 330 m apart and the stations are alternating BBMT or audio-magnetotelluric (AMT) data, the latter having a frequency range of 1–10,000 Hz and occupation times of two to four hours. These data are used to estimate the resistivity (or conductivity) as a function of depth beneath the transects, ideally to depths up to 75 km.

Gravity data were also acquired along the transects with a station spacing of approximately 300 m (Maleki et al., 2021). Finally, density and magnetic susceptibility measurements were taken from hand samples and outcrops, respectively, to constrain the gravity and magnetic modeling (Eshaghi et al., 2019; McNeice et al., 2022). Drill-hole logging has also been undertaken.

Example applications

As an example of how the geophysical data have provided geologic insight into the crustal structure and endowment of certain areas, we will review the results from three transects. The results from these transects have been published recently and provide interesting and diverse inferences.

Noranda transect. The Noranda area is dominated by mafic and felsic metavolcanic rocks of the Blake River assemblage and synvolcanic intrusions (Figure 2). The southern and northern boundaries of these rocks are demarcated by major transcrustal faults (marked with thick red dashed lines labeled the Porcupine-Destor Fault [PDF] to the north and the Cadillac-Larder Lake Fault [CLLF] to the south), with several minor faults between them that dissect the volcanic stratigraphy and divide it into a number of structural blocks (thick black dashed lines). The Noranda transect is marked with a dotted turquoise line that is largely parallel to the seismic transect marked with a dark-green solid line. These two lines are as indicated in the bottom right of the map legend. Near the southern end, the transect crosses

the Horne Creek Fault, close to two gold-rich deposits containing primarily copper and zinc. These are the Horne mine (labeled I) and the Quémont mine (labeled II), both marked with orange circles. Both are volcanogenic massive sulfide (VMS) deposits. Gold mines and former gold mines to the east, west, and south are marked with yellow circles, many of which occur close to the transcrustal CLLF to the south and the PDF to the north. Close to the transect and the Lac Dufault pluton (and at a number of other locations) are red dots, marking the locations of other VMS deposits.

The sections derived from the geophysical data can be used to infer the structure below the surface geology. The reflection seismic data section is shown in Figure 3b, with the areas S1 and S2 contained within the dashed cyan and dashed light-green lines. These areas display very few laterally coherent reflectors, possibly because the geologic features in this area are primarily vertical or subvertical, are large nonreflective plutonic bodies, or are features smaller than a quarter of the seismic wavelength (15–500 m). These areas are considered upper-crustal rocks, and similar signatures are seen on all the other transects. The area S3 is made up of more laterally extensive subhorizontal reflectors, in this case primarily dipping shallowly to the south. This subhorizontal character is typical of what we term midcrustal rocks. The lower crustal signature is largely similar to that in the midcrust, but on this transect the number of subhorizontal reflectors decreases somewhat toward the Moho depth, estimated at 38 km by Benn (2006) from reflection seismic data.

The density section (Figure 3c), derived from unconstrained inversion of the gravity data, shows less dense rocks in the upper 5 to 10 km, with the lowest density rocks corresponding to the

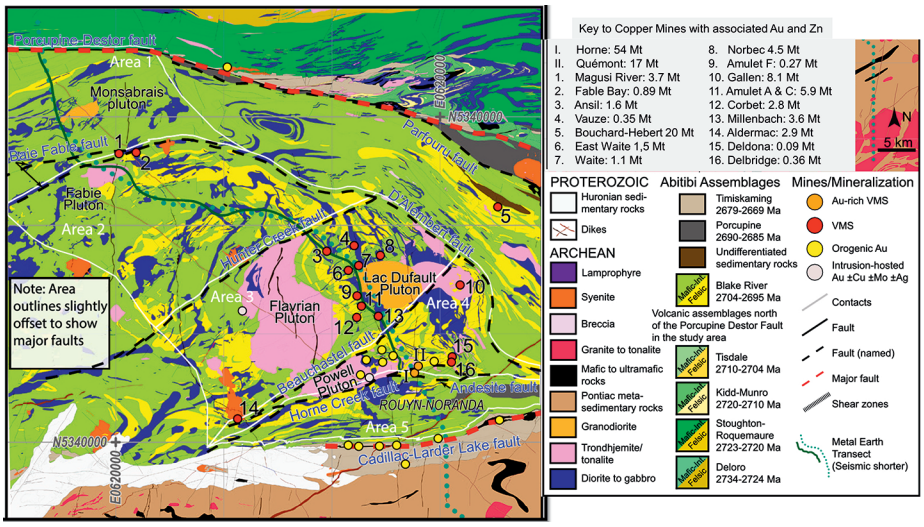

Figure 2. The geology of the Noranda area classified by rock type, with the legend lower right and the key to important mineral deposits above the legend. The area outlines are shown in white. Modified from Jørgensen et al. (2022).

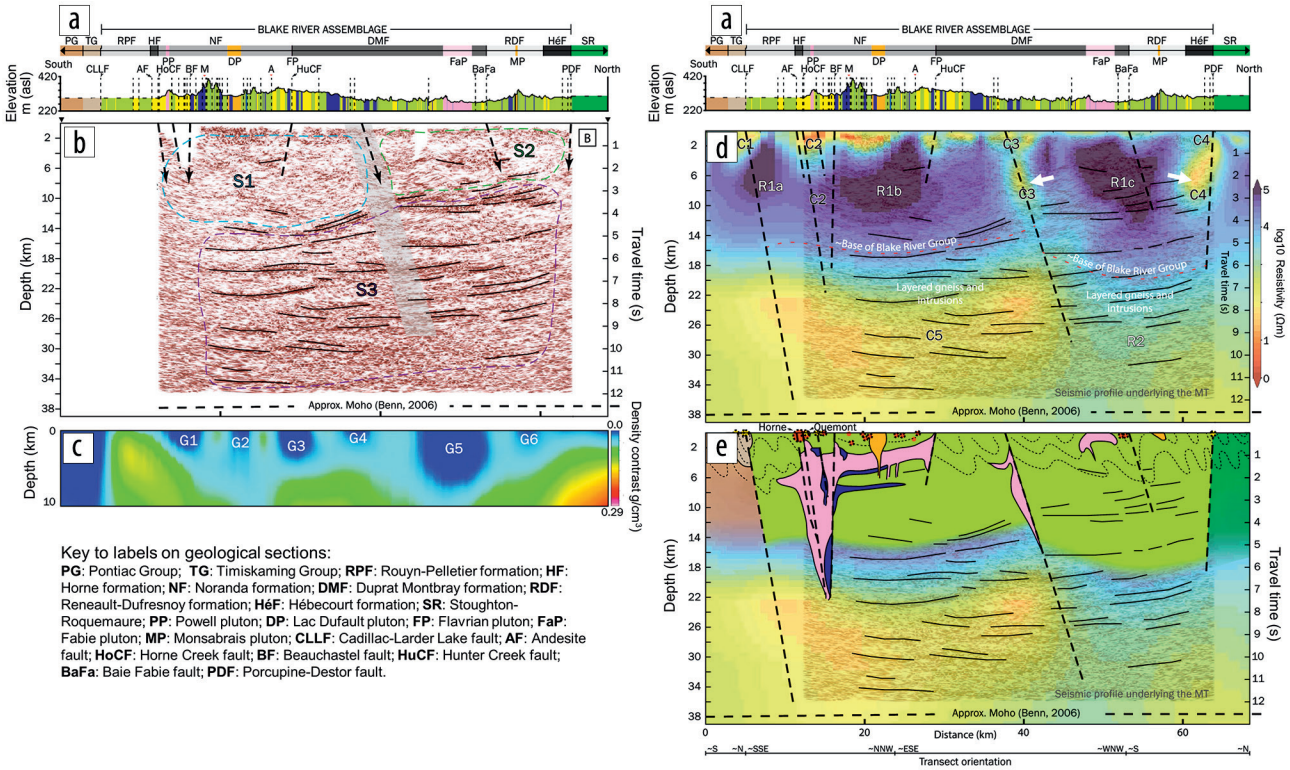

Figure 3. (a) The geology and topography along the Noranda transect, shown left and right above sections derived from (b) the reflection seismic data, (c) gravity data, and (d) MT model overlain on the seismic data. The geologic interpretation is shown in panel (e). Modified from Jørgensen et al. (2022).

plutons or larger packages of felsic rocks. The resistivity section derived from the MT data is shown as color in Figure 3d, with the seismic data and seismic interpretation shown as an overlay. The MT model has identified three resistive zones in the upper crust. Zones R1a and R1b lie within seismic zone S1. Resistive zone R1c is within S2, but there is a slightly less resistive zone extending to greater depth below S2, which has been interpreted to comprise rocks of the Blake River group (the base of which is marked with the red dashed line). Two conductive zones labeled C3 (left white arrow) seem to define a conductive zone extending from surface to the midcrust. Within the midcrust, it separates a large conductive zone to the south, labeled C5, from more resistive material to the north. This C3 zone has been marked in gray on the seismic section. It corresponds with a cusp in the upper to midcrust boundary and the termination of some mid-crustal reflectors. A similar conductive zone C4, marked with the right white arrow, appears near the PDF at the extreme north of the section. The other major crustal structure, the CLLF only has a very near-surface conductive zone (C1), as does the Horne Creek Fault, which is labeled C2. There are a number of other near-surface conductive zones above C5 without the same strong connection to the midcrust as C3 and C4. These geophysical sections (B to D) were used to help construct the interpreted section shown in Figure 3e.

The conductive zones C3 and C4 (highlighted with white arrows) could be interpreted as pathways where hydrothermal fluids migrated to the surface from deeper in the earth. This interpretation is similar to the interpretation made by Heinson et al. (2018) when subvertical conductive features were identified connecting the giant Olympic Dam orebody with a conductive zone in the midcrust. However, the 2D section in Figure 3d fails to show an obvious pathway associated with the significant Horne and Quémont deposits. Note however, that Figure 3d is a 2D section taken from a larger 3D model: the MT station locations are primarily along the transect, but there are other legacy MT stations away from the transect (Roots et al., 2022). These stations have been used to generate a 3D model using the HexMT inversion algorithm (Kordy et al., 2016a, 2016b). A 3D view of the results around the Noranda area is shown in Figure 4. The 3D perspective view in Figure 4a shows that the C5 conductor at about 20 km depth is laterally extensive, and many of the conductive pathways that come to surface are not vertical but start at 20 km depth, move away horizontally from C5, then curve upward and frequently head back in the opposite horizontal direction nearer the surface. For example, in Figure 4a, feature C1 (on the far right) moves out to the right from C5, up, and then back to the left at surface, while C3 moves out to the left, up, and then back to the right. This suggests that some of the near-surface features in Figure 3d might be fed by zones that are out of the 2D section. Figure 4b is a plan view of the resistivity at 5.5 km depth, with north to the top. The Horne and Quémont mines are near the center of the black section line A-A', where the rock is resistive at 5.5 km depth. This resistive zone at 5.5 km below Horne/Quémont is also evident on the section (Figure 4c); however, the conductive zone C2 near these mines and the deep conductive zone (C5) are clearly linked by a zone that moves to the east and then curls back in again. This example illustrates the importance of 3D inversion and 3D imaging in identifying pathways feeding mineralized zones.

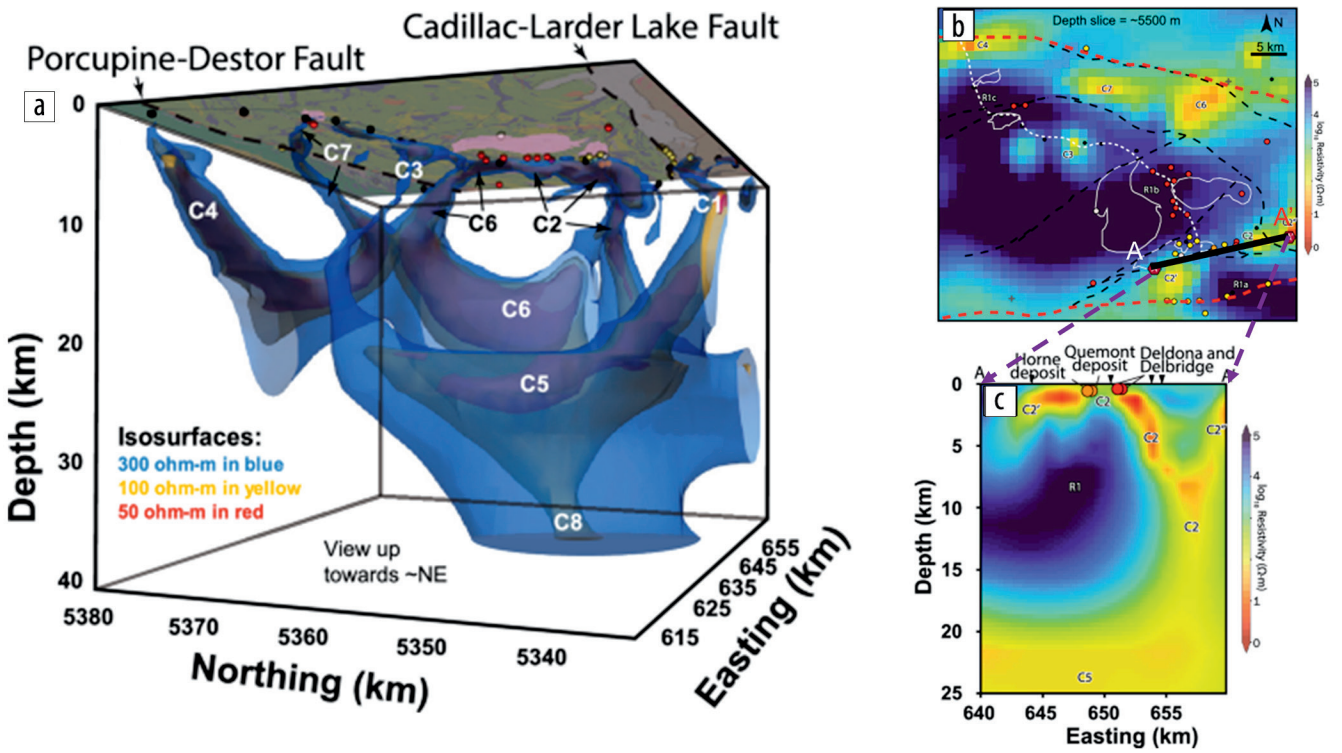

Figure 4. (a) The resistivity section derived from the MT data shown in perspective view looking toward the northeast, (b) plan view at 5.5 km depth, with the location of section line A-A' shown in black, and (c) a section view along A-A'. Modified from Jørgensen et al. (2022).

Matheson transect. The distinctive feature on the seismic reflection data along the Matheson transect (Figure 5a) is a zone of low reflectivity between two interpreted major faults (dashed lines) associated with discontinuous reflectors (indicated with arrows). The upper crust (above about 10 km) does not show many reflections, just like the Noranda transect. On the resistivity section (Figure 5b), which is about 50 km longer than the seismic section, this low-reflectivity zone coincides with a conductive feature, C1, emanating from a laterally larger conductive feature to the south. The mineralized rocks at Matheson are associated with the PDF, which separates the Porcupine assemblage (gray in Figure 5) from the Lower Tisdale assemblage (Figure 5c). At surface, the PDF dips about 30° to the south (Della Justina and Smith, 2020). However, the deeper geophysics on Figure 5 has the PDF interpreted to steepen (Figure 5c), and the material between the two black dashed lines appears to be nonreflective and conductive, inferring possibly a hydrothermal alteration zone that could have been a mineralizing fluid pathway.

At Matheson, more detailed high-resolution seismic data and AMT data were acquired along a shorter part of the section labeled A-A' on Figure 5b and outlined with a black box. The final geologic interpretation of these data is shown on Figure 6 in a perspective view. An additional feature evident on the high-resolution seismic data is what is tentatively interpreted as the top of the Deloro assemblage, a package of volcanic rocks and banded iron formations (BIFs) that are older than the Tisdale assemblage. The 3D reflection package associated with this feature in the Matheson area is shown in Cheraghi et al. (2022a). Haugaard et al. (2021) hypothesize that this reflector may be a BIF at about 7.5 km depth, as BIFs occur elsewhere in the Abitibi very near the top of the Deloro. This reflector is labeled SR9 on the dark-gray seismic section shown in Figure 7a. Della Justina (2022) looked at three other parallel seismic sections in the Matheson area and identified a similar reflector on these sections, labeled SR7, SR5, and SR3 (Figure 7a). If these reflections are part of the Deloro assemblage, then the shallowing that is evident to the west should have a corresponding signature in the gravity data, as the felsic volcanic-dominated Deloro is less dense than the overlying mafic volcanic-dominated Lower Tisdale assemblage. To overcome the inherent nonuniqueness in gravity modeling, the geometry of the sedimentary-dominated Porcupine assemblage, which is also less

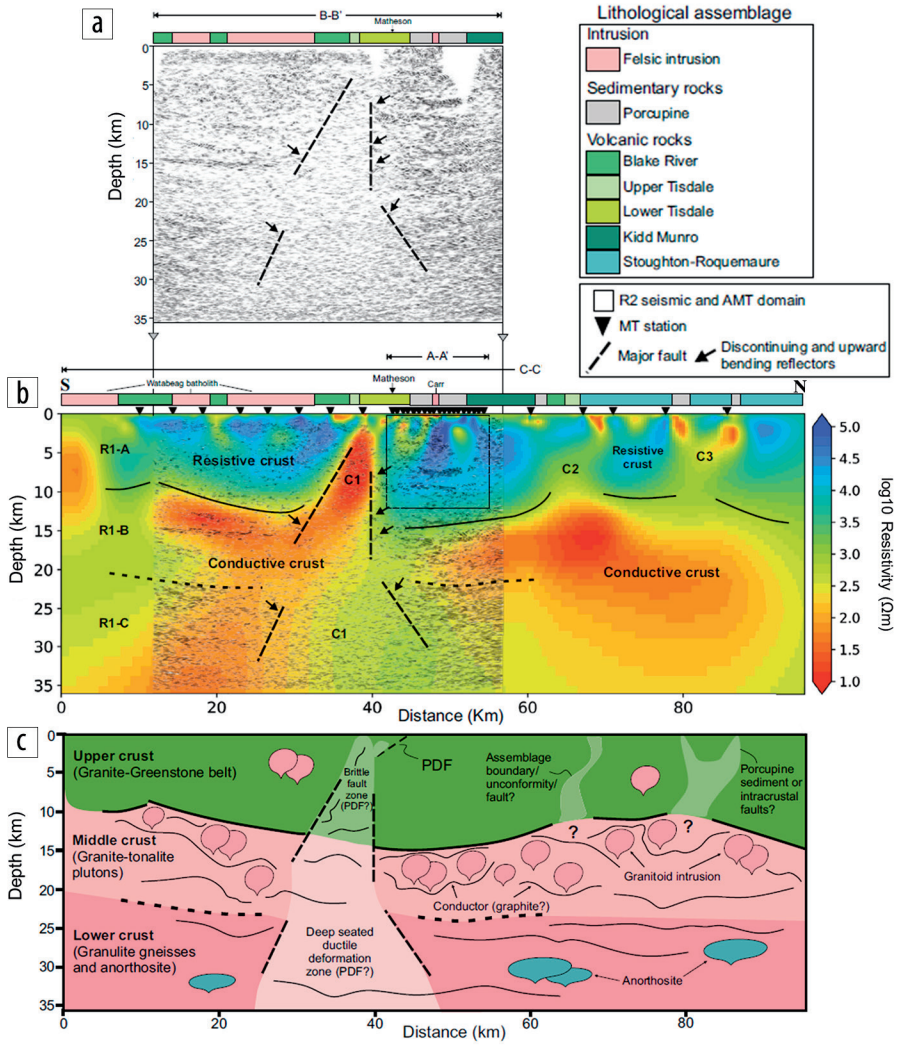

Figure 5. (a) The seismic section from the Matheson transect below the surface geology with the geologic legend on the right. (b) The resistivity section derived from the MT data for a longer transect at Matheson with the seismic shown as an overlay. (c) The geologic section interpreted from the data. Modified from Haugaard et al. (2021).

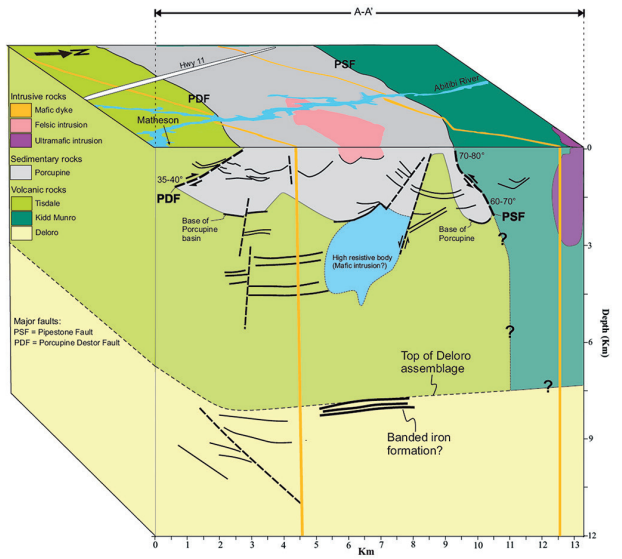

Figure 6. Geologic interpretation of the high-resolution section A-A'. Modified from Haugaard et al. (2021).

dense relative to the Lower Tisdale assemblage, was determined by 2D forward modeling constrained by seismic reflectors interpreted as the base of the Porcupine (Figure 7b). The geometry of the Porcupine was then fixed in a subsequent 3D inversion. The resulting 3D model (Figure 7c) is consistent with the gravity data (rms misfit of 1 mGal, which is comparable to the gravity reading error) and the seismic interpretation and shows the Deloro shallowing to the west. This shallowing is consistent with the mapped geology, as the Deloro outcrops even further to the west. This example shows that gravity modeling can be used to confirm seismic interpretations and resolve deep structure if the shallower structure is constrained.

Larder Lake transect. Passive seismic data were collected on the Larder Lake transect in addition to the active-source reflection data (Naghizadeh et al., 2022). The reflection seismic data are shown in section in Figure 8 as a 3D perspective view looking from the east, and the geology to the west of the transect is shown above the traverse line. On the section, the well-endowed CLLF is inferred as a subvertical fault that terminates a large number of midcrustal reflectors to the north of the fault. The Lincoln-Nipissing Fault is less obvious to the south, but some weakly mineralized faults to the north (the Mulvan Lake Fault and the Misma-Mist Lakes Fault) are inferred from terminations of the subhorizontal events marked with the dotted green lines, particularly at shallow depths. The hatched zone marked M2 is a zone of low reflectivity that Naghizadeh et al. (2022) interpreted as a fossilized magma pathway.

The passive data were processed to extract two sections. The P-S convertibility section that incorporates all frequency bands is shown in Figure 9. The strongest positive amplitude (red) feature

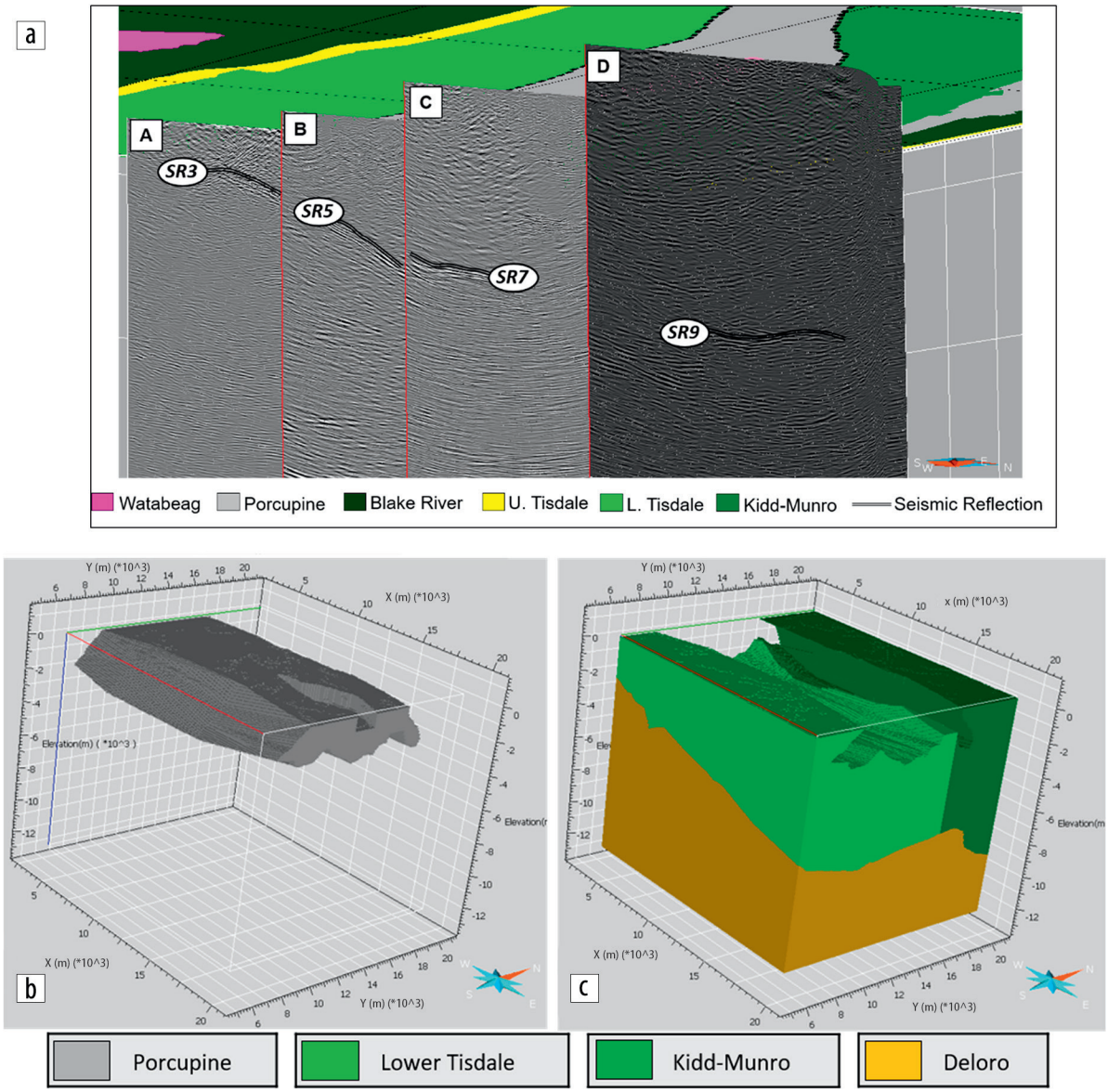

Figure 7. (a) The four seismic sections in the Matheson area shown in perspective view (viewed from below) from the southeast, beneath the surface geology. (b) A perspective view of the Porcupine assemblage as determined from forward gravity modeling and fixed in the 3D modeling, viewed from above. (c) The inverted 3D gravity model, viewed from the same perspective as (b), showing the Deloro shallowing to the west. Modified from Della Justina (2022).

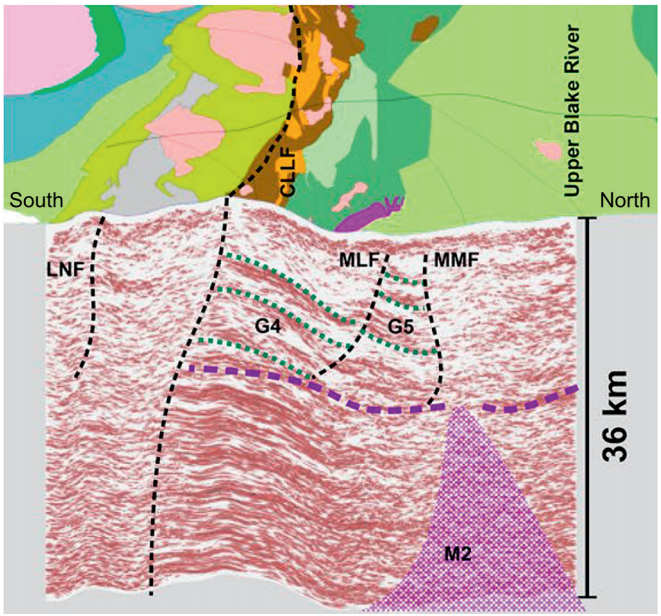

Figure 8. Reflection seismic section shown as a perspective view from the east, with the geology to the west of the transect shown above. Labels G4 and G5 indicate reflective zones and the dashed purple line is the interpreted boundary between the upper and midcrust. Modified from Naghizadeh et al. (2022).

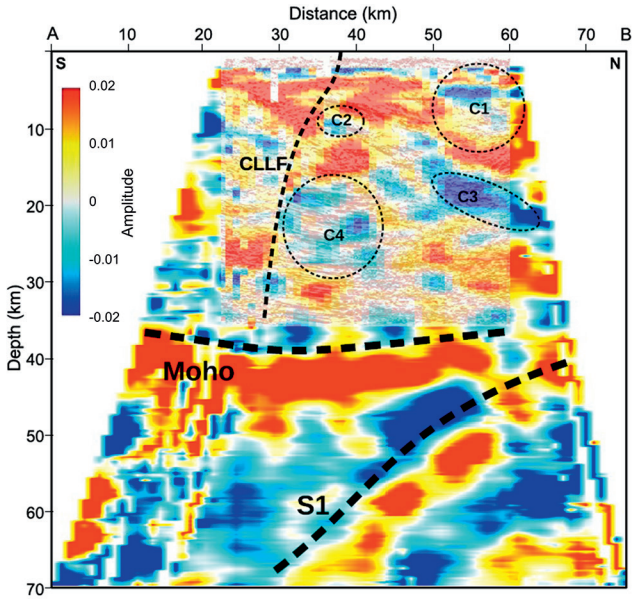

Figure 9. The P-S convertibility section for Larder Lake from the receiver function analysis of the passive seismic data. This image is an average of all the frequency bands. Hotter colors are positive convertibility amplitudes, and cooler colors are negative. C1 to C4 are zones of negative convertibility. From Naghizadeh et al. (2022).

is interpreted to be the base of the Moho, just below the bottom of the reflection seismic section, which is shown as an overlay. Another feature, S1, dipping to the south is also evident in a more regional study documented by Snyder et al. (2021). Naghizadeh et al. (2022) ascribe this feature to a part of the crust delaminating from the base, a slab of oceanic material, or a fault, whereas Snyder et al. (2021) assert it is unlike a modern plate-tectonic subduction zone and hypothesize an association with a later Precambrian event. Shallower features labeled C2 and C4 are terminated by the CLLF and so are consistent with the reflection seismic data, but the red zone above C2 is not. Zone C4 is below a strong reflector.

The shear-wave velocity data derived from the ambient-noise surface-wave tomography are shown in Figure 10b and are compared with the reflection seismic data (Figure 10a) and the P-S convertibility section (Figure 10c) for the top 10 km. The convertibility section here only shows the highest frequency band in order to highlight sharper features. The three models are all broadly consistent. The strong contrasts in the shear-wave velocity in Figure 10b would imply a corresponding contrast in the P-wave velocity. Depending on the

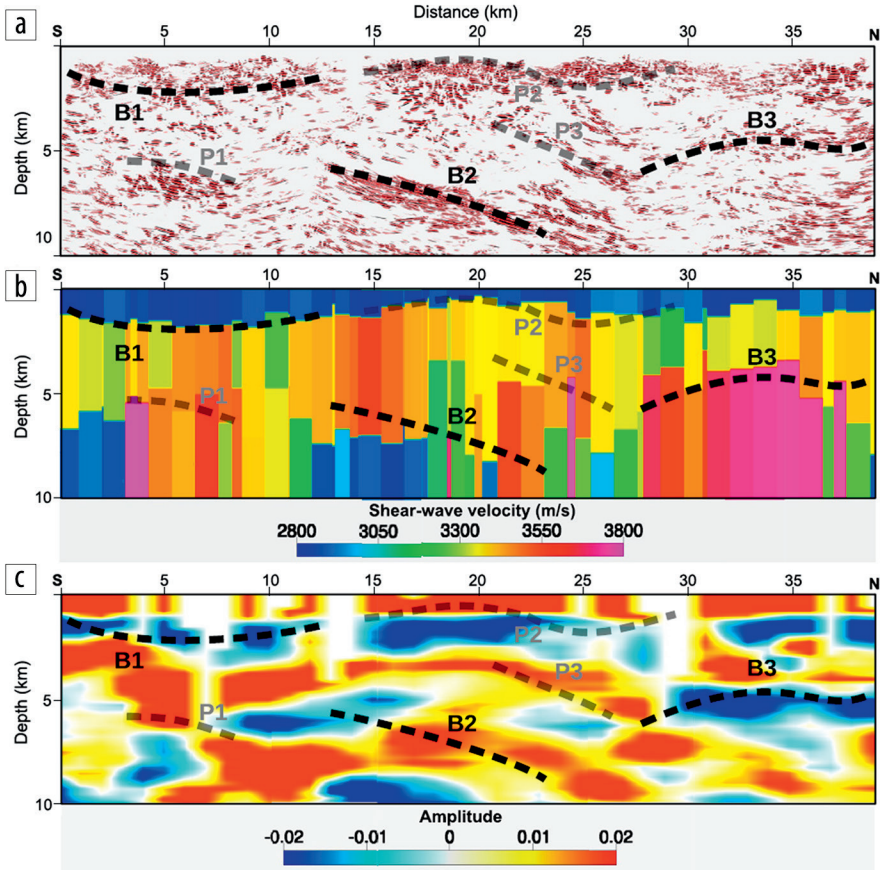

Figure 10. A comparison of the shallow active and passive seismic data at Larder Lake. (a) The reflection seismic data, (b) the shear-wave velocity data from the ambient-noise surface-wave tomography, and (c) the P-S convertibility section, in this case for the highest-frequency band. From Naghizadeh et al. (2022).

density, the acoustic impedance contrast should be strong, so the presence of reflectors at B1 to B3 in Figure 10a is not surprising. On the convertibility section (Figure 10c), B1 to B3 coincide with strong features, although sometimes the location coincides with a transition in convertibility (B2) and sometimes an extreme (B3 is a strong positive and B1 is a strong negative). However, this uncertainty is not unexpected given the diffuse nature of convertibility sections. Three other features P1, P2, and P3, show a somewhat poorer agreement across all three sections.

These seismic sections show that the passive data can provide confirmatory and complementary information, for example providing velocity information in the gaps between reflection events. However, the differing bandwidths of the three different methods, and hence different resolutions, make the sections somewhat problematic to compare. There are similar bandwidth and resolution issues when comparing seismic-reflection sections and MT models.

Other transects. Similar workflows and interpretation procedures have been followed for the other transects shown in Figure 1, with geophysical results published for the Chibougamau transect (Matthieu et al., 2020), the Chicobi transect (Zhou et al., 2021), which is a short 12 km transect north of the Malartic transect, and the Sturgeon Lake greenstone belt transect (Ma et al., 2021). A related study is of the Temagami magnetic anomaly (Adetunji et al., 2021), the source of which is believed to be deep and is poorly understood. Adetunji et al. (2021) introduce recent drilling information and have reinterpreted the MT data to conclude that there is an intrusion that is potentially enriched in nickel-copper-platinum-group elements and might have contributed to the metal endowment of the Sudbury Igneous Complex.

Method development

In addition to the application of geophysical studies for understanding the geologic setting of mineral deposits, research has also been undertaken to improve the methodologies used in geophysical studies.

The collection of BBMT and AMT data on high-resolution lines and broadband data on the regional lines created a computing issue: the fine meshes required to define the resistivity structure in the high-resolution areas could not be used for the regional model because the size of the resulting model was too large for the supercomputing clusters used to invert the data. The methodology developed to deal with this issue (Hill et al., 2021) was to invert the regional model first on a coarse scale and then transfer this regional model to a finer mesh and use it as the starting model and (optionally) the reference model for the inversion of the high-resolution data.

Much of the effort in seismic method development revolved around dealing with the fact that the reflection seismic lines are crooked and the geology is often not perpendicular to strike. When 2D processing methods are applied to crooked-line data, this can result in images with few coherent reflections. However, the crooked lines can also be used to extract 3D information and improve the imaging. One approach, described by Villamizar et al. (2022), incorporates a velocity model derived from full-waveform inversion of the reflection seismic data and stacks the data in a direction dependent on the a priori geologic strike. Although the velocity model was only well constrained in the top 3 km, the imaging of deeper structures was more coherent.

Cheraghi et al. (2020, 2021, 2022a, 2022b) tried a number of different combinations of seismic processing methods to get the best results on a number of crooked high-resolution detailed transects. The methods tested include prestack dip moveout (DMO), cross-dip moveout (CDMO) analysis, Kirchhoff prestack time migration (PSTM), Kirchhoff prestack depth migration (PSDM), coherency migration, and even 3D processing applied to 2D crooked geometries. Some of the major challenges along Metal Earth high-resolution seismic transects are the crooked geometry and irregular common-midpoint (CMP) distribution; out-of-plane reflections; scattering and low signal-to-noise ratio; and complex subsurface architecture hosting several fault and fold systems. These challenges have been addressed and appropriate seismic imaging solutions have been presented (see Cheraghi et al., 2020, 2021, 2022a, 2022b). The researchers adapted a processing flow to increase the coherency of the imaged reflections in the upper crust (down to depths of 12 km). One innovative aspect of Cheraghi et al. (2021, 2022a) was to investigate the effect of survey geometry (irregular CMP distribution) and its effect on application of common-offset DMO and PSTM (acquisition footprint), a matter that has been less studied in crystalline rock environments. Also, coherency migration, an advanced imaging method based on PSDM, has been tested on Metal Earth high-resolution transects (Cheraghi et al., 2022b). This method has been applied successfully only in a few research areas in crystalline rock environments (see Cheraghi et al., 2022b, and references therein). Overall, the results obtained depend on the geometry of the profiles and complexity of subsurface geology, with different conclusions drawn at Swayze (Cheraghi et al. 2020), Chibougamau (Cheraghi et al., 2021), Matheson (Cheraghi et al., 2022a), and Swayze East (Cheraghi et al., 2022b). In addition, Mancuso and Naghizadeh (2021) have developed a generalized CDMO correction and applied it to the Larder Lake transect. Compared with conventional processing, the new method showed an increased coherency of reflections that were also more compatible with the known surface geology of the study area.

Yet another approach to dealing with the crooked-line processing problem is a 2.5D multifocusing method developed by Jodeiri Akbari Fam et al. (2021, 2022). This method combines multiple nearby CMP gathers into a supergather and then solves an inversion problem to estimate the wavefield parameters of the reflection surface. This step provides a number of seismic attribute sections. The subsequently stacked data then can be migrated to provide a final section. Figure 11a shows the normal CMP processing with only one zone having somewhat coherent reflections (the zone inside the dashed box). After phase-shift time migration (Figure 11b), this zone is more coherent (the zone labeled L5). A small dipping reflector also becomes coherent at L4, and there is a slight improvement at L0 and L3. At the northwest end of this migrated CMP section, there are essentially no features imaged. The 2.5D multifocused section (Figure 11c) shows stronger coherence in the same dashed box. After migration, this zone appears larger than that in Figure 11b. In Figure 11d, the poststack

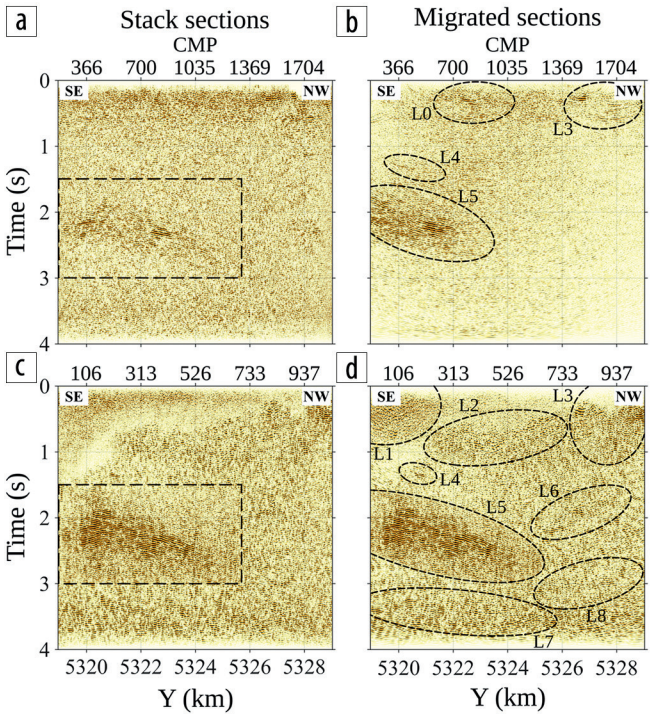

Figure 11. Comparison of standard 2D processing with 2.5D multifocusing on the Larder Lake section. (a) CMP stacked section, which includes a normal moveout and DMO assuming a straight transect. (b) Phase-shift time-migrated CMP-stacked section of (a). (c) 2.5D multifocusing stack along a smoothed crooked line. (d) Poststack Kirchhoff time migration of (c). From Jodeiri Akbari Fam et al. (2022).

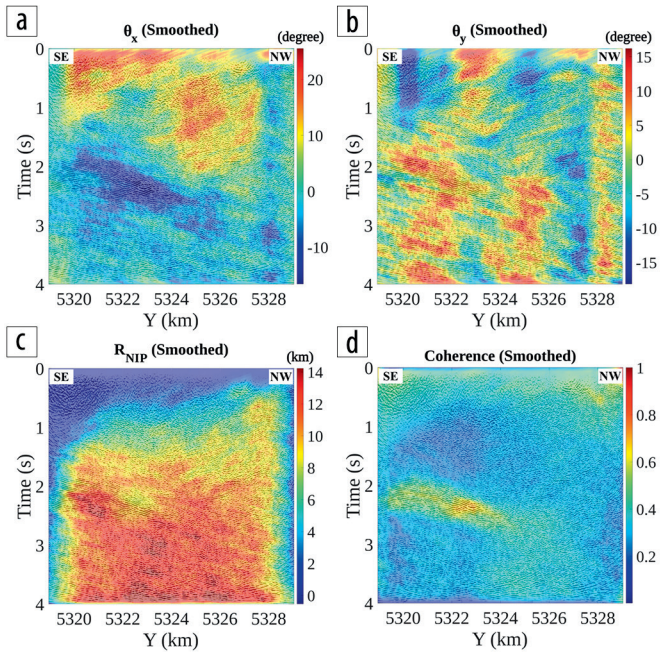

Figure 12. Seismic attribute sections. (a) The apparent dip along the north-south direction (red to the south, blue to the north). (b) The apparent dip along the east-west direction (red to the east, blue to the west). (c) The radius of the normal-incident-point wave curvature. (d) The coherence section, an indicator of how coherently the traces in the supergather stack. The 2.5D multifocusing stack section is shown as a black-and-white overlay. From Jodeiri Akbari Fam et al. (2022).

Kirchhoff time migration of Figure 11c, a dipping reflector at L4 becomes evident, albeit in a slightly different place, while the zone at L3 is slightly more reflective. However, in Figure 11d there is nothing evident at L0, suggesting that that feature in Figure 11b might be an artifact. There are new or stronger features evident in Figure 11d at L2 that appear to show a dip to the southeast. Four zones (L1, L2, L6, L7, and L8) all show reflections that are not evident in Figure 11b.

The wavefield parameters derived from the inversion in the 2.5D multifocusing are shown in Figure 12. The apparent dip is the dip of the reflection surface, which can be in any direction, so it is decomposed into two orthogonal directions (north-south and east-west). The apparent dip in the north-south direction (Figure 12a) shows southward dips in red and northward dips in blue. For a specific supergather, e.g., around 5326 km (northing), the dip is to the south in zone L6, but at a later two-way traveltime in the same supergather, the dip of the reflection surface is to the north. Zone L1 is interesting in that the dip in the south part is to the north and the north part is to the south, suggesting a syncline. The cross-dip image (Figure 12b) shows the eastward dip as red and the westward dip as blue. Zone L1 and zone L2 change from red in the south to blue in the north (suggesting some type of strike rotation or scissoring) and zone L5 is predominantly red. The R_{NIP} section (Figure 12c) shows the radius of curvature at the normal incident point on the reflection surface for that supergather at that two-way traveltime. The radius of curvature generally increases with depth, but subtle changes are evident, particularly in zone L5. The coherence section (Figure 12d) is a measure of how well the individual traces in each supergather stack together for the wavefield parameters selected by the inversion, so this is a measure of confidence in the inversion results (equivalent to data fit). Zone L5 has the greatest coherence, but L1 is also high, suggesting that the synclinal feature can be interpreted with confidence.

Discussion and conclusions

The Metal Earth geophysical data have contributed to extending the mapped geology to depth and on either side of the transect (primarily the gravity and magnetics) and have helped identify large-scale faults at surface that may be mineralized structures.

The gravity data have helped identify interfaces at depths of up to 7 or 8 km. In some cases, the overlying density had to be constrained using physical properties measurements and other interfaces fixed using seismic reflection data.

The MT data were useful for identifying resistive upper crust and determining locations where the midcrust is conductive. In many cases, zones that are well endowed with mineral deposits are associated with more conductive chimneys connecting a conductive part of the midcrust with the mineralized zones. These zones were not always evident on 2D sections because they were sometimes in or out of the profile. This highlights the importance of 3D modeling and, by inference, the acquisition of 3D data.

The reflection seismic data show low reflectivity in the upper crust and subhorizontal reflectors in the midcrust. Zones for the transportation of mineralizing fluids that may transport metals to the depositional sites are sometimes, but not always, associated

with zones of low reflectivity, suggesting the rocks have been hydrothermally altered or deformed in some way. Mineralizing structures can sometimes be identified as truncations of subhorizontal reflectors, particularly if the structures extend to the midcrust, or the reflectors are evident in the upper crust.

Passive seismic data provide a useful complement to the reflection seismic data, with the ambient-noise surface-wave tomography able to quantify the shear-wave velocity between some of the stronger reflectors and the receiver function analysis able to identify large-scale features at much greater depth than the reflection survey we acquired. The different bandwidths and resolutions make comparing the three types of seismic data sets difficult.

Active-source seismic reflection data provided the most continuous, high-resolution image of subsurface structure. The velocity anomalies, conductors, and P-S conversions generated from the passive data do indeed provide additional information, but they almost always require reflectors for spatial context. The passive seismic features would be very cryptic if interpreted in isolation, as the images look somewhat like a checkerboard. The MT conductors, although also somewhat lower in resolution, can provide important complementary information, particularly for subvertical features.

New tools have been developed for processing and interpreting crooked-line seismic surveys in hard-rock terrains, with an improvement in the quality of the images and the sections that can be interpreted.

The results we have presented here are from the initial phase of the project, which involved data collection and integration on each transect individually. This work was undertaken by a number of different researchers, so the interpretations, for example those in Figures 3e and 5c, have a different style, although the data acquired are the same. The current phase of the project is to systematically compare the different transects to understand the characteristics of the well-endowed traverses compared with the other traverses and use this to identify well-endowed areas and devise methodologies to look for critical mineral deposits. TLE

Acknowledgments

The authors would like to acknowledge the diverse and significant contributions to the geoscience community from the late Phil Wannamaker prior to his sudden death. We are particularly grateful that he was able to contribute to this specific work. We are also grateful for contributions from SAExploration, Absolute Imaging, Complete MT Solutions, Moombarriga Geoscience, and Sisprobe for acquisition and processing of the data; Mira Geoscience, AspenTech, Seequent, Adobe, and Esri for providing software; and finally to the Canada First Research Excellence Fund for funding this research. This is Mineral Exploration Research Center/Metal Earth contribution MERC-ME-2022-41.

Data and materials availability

Data are available from https://merc.laurentian.ca/research/metal-earth/public-data or by contacting the corresponding author.

Corresponding author: rssmith@laurentian.ca

References

Adetunji, A., I. J. Ferguson, R. Vayavur, S. Cheraghi, M. Naghizadeh, W. Whymark, R. S. Smith, J. Ayer, and J. A. Craven, 2021, Evidence of magmatism and rifting in the southern superior craton from the Temagami geophysical anomaly: Precambrian Research, **362**, 106310, https://doi.org/10.1016/j.precamres.2021.106310.

Ammon, C. J., 1991, The isolation of receiver effects from teleseismic P waveforms: Bulletin of the Seismological Society of America, **81**, no. 6, 2504–2510, https://doi.org/10.1785/BSSA0810062504.

Benn, K., 2006, Tectonic delamination of the lower crust during Late Archean collision of the Abitibi-Opatica and Pontiac terranes, Superior province, Canada, *in* K. Benn, J.-C. Mareschal, and K. C. Condie, eds., American Geophysical Union Geophysical Monograph Series 164, 267–282, https://doi.org/10.1029/164GM17.

Campillo, M., 2006, Phase and correlation in 'random' seismic fields and the reconstruction of the Green function: Pure and Applied Geophysics, **163**, no. 2–3, 475–502, https://doi.org/10.1007/s00024-005-0032-8.

Cheraghi, S., F. Hloušek, S. Buske, A. Malehmir, A. Adetunji, R. Haugaard, D. Snyder, and R. Vayavur, 2022b, Reflection seismic imaging across a greenstone belt, Abitibi (Ontario), Canada: Geophysical Prospecting, https://doi.org/10.1111/1365-2478.13284.

Cheraghi, S., A. Malehmir, M. Naghizadeh, D. B. Snyder, L. Mathieu, and P. Bedeaux, 2021, Seismic imaging across fault systems in the Abitibi greenstone belt — An analysis of pre- and post-stack migration approaches in the Chibougamau area, Quebec, Canada: Solid Earth, **12**, no. 5, 1143–1164, https://doi.org/10.5194/se-12-1143-2021.

Cheraghi, S., A. Malehmir, R. Vayavur, P. Shamsipour, M. Naghizadeh, R. Haugaard, D. B. Snyder, and J. Ayer, 2022a, Addressing geometrical attributes and seismic imaging capability of fault systems in a world-class metal endowed region: Abitibi greenstone belt, Canada: Tectonophysics, **833**, 229361, https://doi.org/10.1016/j.tecto.2022.229361.

Cheraghi, S., M. Naghizadeh, D. Snyder, R. Haugaard, and T. Gemmell, 2020, High-resolution seismic imaging of crooked two-dimensional profiles in greenstone belts of the Canadian shield: Results from the Swayze area, Ontario, Canada: Geophysical Prospecting, **68**, no. 1, 62–81, https://doi.org/10.1111/1365-2478.12854.

Della Justina, F., 2022, The incorporation of geophysical, petrophysical and geological constrains in gravity modeling to resolve structures at depth: PhD thesis, Laurentian University.

Della Justina, F., and R. Smith, 2020, 2D forward gravity and magnetic modeling of the Porcupine assemblage, Matheson area: 90th Annual International Meeting, SEG, Expanded Abstracts, 999–1003, https://doi.org/10.1190/segam2020-3427249.1.

Eshaghi, E., R. S. Smith, and J. Ayer, 2019, Petrophysical characterization (i.e. density and magnetic susceptibility) of major rock units within the Abitibi greenstone belt: Laurentian University Mineral Exploration Research Centre, publication number MERC-ME-2019-144.

Haugaard, R., F. D. Justina, E. Roots, S. Cheraghi, R. Vayavur, G. Hill, D. Snyder, J. Ayer, M. Naghizadeh, and R. Smith, 2021, Crustal-scale geology and fault geometry along the gold endowed Matheson transect of the Abitibi greenstone belt: Economic Geology and the Bulletin of the Society of Economic Geologists, **116**, no. 5, 1053–1072, https://doi.org/10.5382/econgeo.4813.

Heinson, G., Y. Didana, P. Soeffky, S. Thiel, and T. Wise, 2018, The crustal geophysical signature of a world-class magmatic mineral system: Scientific Reports, **8**, no. 1, 10608, https://doi.org/10.1038/s41598-018-29016-2.

Hill, G. J., E. A. Roots, B. M. Frieman, R. Haugaard, J. A. Craven, R. S. Smith, D. B. Snyder, X. Zhou, and R. Sherlock, 2021, On Archean craton growth and stabilisation: Insights from lithospheric resistivity structure of the Superior Province: Earth and Planetary Science Letters, **562**, 116853, https://doi.org/10.1016/j.epsl.2021.116853.

Jodeiri Akbari Fam, H., M. Naghizadeh, R. Smith, O. Yilmaz, S. Cheraghi, and K. Rubingh, 2022, High-resolution 2.5D multifocusing imaging

of a crooked seismic profile in a crystalline rock environment: Results from the Larder Lake area, Ontario, Canada: Geophysical Prospecting, https://doi.org/10.1111/1365-2478.13285.
Jodeiri Akbari Fam, H., M. Naghizadeh, and O. Yilmaz, 2021, 2.5 D multifocusing imaging of crooked-line seismic surveys: Geophysics, **86**, no. 6, S355–S369, https://doi.org/10.1190/geo2020-0660.1.
Jørgensen, T. R. C., H. L. Gibson, E. A. Roots, R. Vayavur, G. J. Hill, D. B. Snyder, and M. Naghizadeh, 2022, The implications of crustal architecture and transcrustal upflow zones on the metal endowment of a world-class mineral district: Scientific Reports, **12**, no. 1, 14710, https://doi.org/10.1038/s41598-022-18836-y.
Kordy, M., P. Wannamaker, V. Maris, E. Cherkaev, and G. Hill, 2016a, 3-D magnetotelluric inversion including topography using deformed hexahedral edge finite elements and direct solvers parallelized on SMP computers — Part I: Forward problem and parameter Jacobians: Geophysical Journal International, **204**, no. 1, 74–93, https://doi.org/10.1093/gji/ggv410.
Kordy, M., P. Wannamaker, V. Maris, E. Cherkaev, and G. Hill, 2016b, 3-dimensional magnetotelluric inversion including topography using deformed hexahedral edge finite elements and direct solvers parallelized on symmetric multiprocessor computers — Part II: Direct data-space inverse solution: Geophysical Journal International, **204**, no. 1, 94–110, https://doi.org/10.1093/gji/ggv411.
Ma, C., M. Naghizadeh, A. Adetunji, R. W. D. Lodge, D. Snyder, and R. Sherlock, 2021, Imaging Neoarchean crustal structures: An integrated geologic-seismic-magnetotelluric study in the western Wabigoon and Winnipeg River terranes, Superior craton: Precambrian Research, **364**, 106339, https://doi.org/10.1016/j.precamres.2021.106339.
Maleki, A., R. Smith, E. Eshaghi, L. Mathieu, D. Snyder, and M. Naghizadeh, 2021, Potential-field modelling of the prospective Chibougamau area (northeastern Abitibi subprovince, Quebec, Canada) using geological, geophysical, and petrophysical constraints: Canadian Journal of Earth Sciences, **58**, no. 3, 297–312, https://doi.org/10.1139/cjes-2019-0221.
Mancuso, C., and M. Naghizadeh, 2021, Generalized cross-dip moveout correction of crooked 2D seismic reflection surveys: Geophysics, **86**, no. 4, V285–V298, https://doi.org/10.1190/geo2020-0278.1.
Mathieu, L., D. B. Snyder, P. Bedeaux, S. Cheraghi, B. Lafrance, P. Thurston, and R. Sherlock, 2020, Deep into the Chibougamau area, Abitibi greenstone belt: Structure of a Neoarchean crust revealed by seismic reflection profiling: Tectonics, **39**, no. 7, e2020TC006223, https://doi.org/10.1029/2020TC006223.
McNeice, W., R. S. Smith, and E. Eshaghi, 2022, How magnetic susceptibilities measured on outcrops can be used for modelling (and constraining inversions of) aeromagnetic data: Exploration Geophysics, https://doi.org/10.1080/08123985.2022.2082281.
Mole, D. R., P. C. Thurston, J. H. Marsh, R. A. Stern, J. A. Ayer, L. A. J. Martin, and Y. J. Lu, 2021, The formation of Neoarchean continental crust in the south-east Superior Craton by two distinct geodynamic processes: Precambrian Research, **356**, 106104, https://doi.org/10.1016/j.precamres.2021.106104.
Naghizadeh, M., R. Smith, K. Rubingh, R. Sherlock, J. Ayer, B. Lafrance, S. Cheraghi, et al., 2022, Active and passive seismic imaging of the central Abitibi greenstone belt, Larder Lake, Ontario: Journal of Geophysical Research: Solid Earth, **127**, no. 2, e2021JB022334, https://doi.org/10.1029/2021JB022334.
Naghizadeh, M., D. Snyder, S. Cheraghi, S. Foster, S. Cilensek, E. Floreani, and J. Mackie, 2019, Acquisition and processing of wider bandwidth seismic data in crystalline crust: Progress with the Metal Earth project: Minerals, **9**, no. 3, 145, https://doi.org/10.3390/min9030145.
Roots, E. A., G. J. Hill, B. M. Frieman, P. E. Wannamaker, V. Maris, A. J. Calvert, J. A. Craven, R. S. Smith, and D. B. Snyder, 2022, Magmatic, hydrothermal and ore element transfer processes of the southeastern Archean Superior Province implied from electrical resistivity structure: Gondwana Research, **105**, 84–95, https://doi.org/10.1016/j.gr.2021.12.004.
Snyder, D. B., G. Savard, B. A. Kjarsgaard, A. Vaillancourt, P. C. Thurston, J. A. Ayer, and E. Roots, 2021, Multidisciplinary modelling of mantle lithosphere structure within the Superior Craton, North America: Geochemistry, Geophysics, Geosystems, **22**, no. 4, e2020GC009566, https://doi.org/10.1029/2020GC009566.
Villamizar, B. J. G., R. G. Pratt, and M. Naghizadeh, 2022, Seismic imaging of crystalline structures: improving energy focusing and signal alignment with azimuthal binning and 2.5-D full-waveform inversion: Geophysical Journal International, **231**, no. 1, 615–628, https://doi.org/10.1093/gji/ggac208.
Zhou, X., B. Lafrance, M. Naghizadeh, D. B. Snyder, A. Q. Adetunji, R. Vayavur, M. A. Hamilton, and J. A. Ayer, 2021, Crust architecture and structural evolution of a Neoarchean sedimentary basin: Geological and geophysical evidence from Metal Earth Chicobi transect in the Abitibi Subprovince, Superior Province, Quebec, Canada: Precambrian Research, **365**, 106391, https://doi.org/10.1016/j.precamres.2021.106391.